Research on operation characteristics of wind supercharged solar chimney dust haze removal street light

Lu Zuo[a*], Zinan Guo[a], Tian Zhou[a], Chenkai Xiao[a], Long Huang[a],Yunting Ge[b]

[a] College of Energy and Electrical Engineering, Hohai University, Nanjing, China

[b] School of the Built Environment and Architecture, London South Bank University, London, UK

ABSTRACT: To realize distributed dust haze removal in street canyons, a innovative wind supercharged solar chimney dust haze removal street light is proposed. The design couples solar chimney technology with municipal street lighting, utilizing thermal pressure, chimney effect and wind supercharged wheel to power the system, which achieves the dual function of lighting and dust haze removal. Operational testing on a small-scale model showed: the airflow warms up the most in the inlet area, and the model creates updrafts with a dust haze removal effect. The filtration system consists of various filter screens arranged by descending filtration efficiency: HEPA, primary filter cotton, activated carbon and nylon filter screens, with airflow velocity in the flow runner in the opposite order. The average filtration efficiency is positively correlated with the pressure drop and negatively correlated with the overflow airflow. A combination of different material filter screens is more effective than simply increasing the thickness of a single filter screen. A single layer of 10mm primary filter cotton has the highest total mass flow of clean air, reaching 4.18g. HEPA has the highest average filtration efficiency at 93.1%. This innovative approach offers an efficient solution for urban air purification while maintaining street lighting functionality.

Keywords: Solar chimney; Wind supercharged wheel; Urban dust haze removal; Street light; Airflow field characteristics; Filtration efficiency

* Corresponding author.
E-mail address: luzuo@hhu.edu.cn (L. Zuo).

0. Introduction

The accelerated urbanization process in recent years has led to a surge in the number of vehicles on the road in urban areas, which has caused more traffic pollution emissions. Among them, particulate matter (PM) emissions from vehicles increase the concentration of atmospheric aerosols, which in turn trigger the occurrence of urban haze, seriously threatening the health of residents. Alternatively, due to the need to accommodate a larger population, the street canyon structure comprising towering buildings and narrow roads in cities hampers the dispersion of particulate pollutants. This leads to heightened pollution exposure to pedestrians, non-motorized vehicle drivers, and motorists within the street canyons. A common method of removing pollutants or reducing pollutant concentrations is roadway water spraying, which improves air quality. However, roadway water spraying is more water intensive and can be limited in its application for urban areas with severe water scarcity. Sprinklers themselves consume power, and fuel sprinklers also have pollutant emissions. In addition, the eliminating or reduction of pollutants can be realized by modifying the aspect ratio of street canyons, building heights, and roof shapes to improve the ventilation efficiency along street-level areas (Kurppa et al., 2018), but this method will change the original urban planning, posing challenges for implementation. In this paper, a novel solar chimney street light for dust haze removal was proposed by coupling solar chimney technology with municipal street lights, so as to alleviate air pollution in urban street canyons.

In 1982, the world's first solar chimney power plant (SCPP) was successfully built in Manzanares, Spain, and operated for seven years (Haaf et al., 2007) which demonstrates the feasibility of the solar chimney power generation technology. SCPP mainly consists of three components: chimney, collector , and air turbine The cold ambient air is heated by the collector and then converged to the center, which drives the air turbine at the base of the chimney to rotate and generate electricity under the chimney effect, finally discharged from the top of the chimney, enabling the conversion of solar energy to electrical energy.

The research of applying solar chimney technology to urban haze removal is gradually emerging. Compared with the traditional urban haze removal methods, solar chimney haze removal technology offers advantages such as stable and sustainable operation, environmentally friendly production and operation, structural stability, extended service life,, and low maintenance cost (Liu et al., 2021). These merits underscore its potential for further development and application. Lodhi et al. (1999)

proposed spraying cold water at the top of a solar chimney to filter and cool the dusty air in the flow path and send it out of the bottom outlet of the chimney. Consequently, the ambient warm dusty air is drawn into the top of the chimney, establishing a self-driven cycle of purified air. Compared to large-sized raindrops, the fine water mist sprayed in the device is more efficient. Zhou et al. (2015) proposed a solar updraft tower to mitigate urban haze by utilizing a towering chimney to drive the warm dust-haze containing air with dust and haze in the urban heat island upward and transfer it into the atmospheric troposphere. Through performance calculations and cost analyses, it is estimated that several major cities in China would require approximately 9 and 8 installations of 1km-high and 1.5 km-high solar chimney systems, respectively. Cao et al. (2015) proposed a solar-assisted large-scale cleaning system consisting of a large-scale flat-plate solar collector, a chimney, and a filter bank, , for filtering polluted air. Numerical simulations calculated that an air filtration flow rate of 2.64×10^5 m^3/s for the system, which is capable of cleaning a total of 22.4 km^3 of polluted air in a day. In addition, a demonstration solar-assisted large-scale cleaning system was successfully completed in Xi'an, China, in 2018, with a 43×60 m^2 collector and a 60-m-high chimney (Cao et al., 2018). The whole system achieved an average $PM_{2.5}$ filtration efficiency of 73.5% and an air filtration rate of 35 m3/s, leading to a 15% reduction in PM density within the surrounding 10 km^2 (Yodo, 2018). Gong et al. (2017) used an inverted U-type cooling tower instead of the chimney of a conventional SCPP to remove $PM_{2.5}$ and large particles from the ambient airflow by a filtration screen placed at the inlet of the collector, and utilized a water spraying system at the top of the chimney to drive the filtered airflow to cool down and sink back to the vicinity of the ground level. The device can clean up to 69984000 m^3 of air per day. Yang and Li (2020) proposed an inversion solar chimney, which produces the effect of downward airflow ventilation by spraying water at the top of the chimney. Direct air capture devices and fine aerosols are installed at the bottom of the chimney to enable the simultaneous filtration of CO2 and dust haze particles in the ambient air. Hachicha et al. (2023) proposed a hybrid filter-equipped solar chimney power plant designed for air purification by adding air filters on both sides of the collector and chimney. When the air filters are placed close to the entrance of the collector, the hybrid filter-equipped solar chimney generates about 28.3kW of electricity while purifying the outdoor air at a rate of 447.6 m^3/s.

The above summarized solar chimney haze removal technologies can be mainly categorized into the three directions: transferring pollutants to high altitudes, sprinkling

water to reduce dust, and direct filtration by purification devices. These innovative measures have little negative impact on the environment and low operating costs, which provide valuable ideas for solving the urban haze problem and are worthy of further research and practice. However, most of them face challenges related to construction complexity and coverage area, indicating that there is still significant progress needed before they can be widely adopted on a large scale.

There are a considerable number of studies on the operational performance tests of vertical solar chimneys. Chen et al. (2003) constructed a vertical solar chimney test device with a height of 1.5 m, a length of 0.62 m, and a width of 100 mm-600 mm. They investigated the effects of different chimney widths and chimney inclinations on the air flow in the runner. Results indicated that the airflow rate in the runner was directly proportional to chimney width, with maximum airflow achieved at a chimney inclination angle was 45°. Li et al. (2009) built a vertical roof solar chimney with a height of 2 m, a length of 1 m, and a width of 0.4 m-1.2 m. It was found that the natural ventilation is directly proportional to the chimney gap and to the heat flux; the interior airflow rate is directly proportional to the solar radiant intensity and inversely proportional to the chimney gap. Ryan and Burek (2010) constructed three vertical roof solar collector plates with heights of 0.5 m, 1.0 m, and 2.0 m. They found that the airflow rate in the runner is proportional to the chimney width. However, when the aspect ratio is greater than 0.2, backflow may occur and reduce the flow rate. Chow and Zhao (2011) constructed a vertical well test model scaled down to 1/200, the distribution of the differential pressure inside the model was investigated at a constant temperature. They found that the differential pressure at the inlet of the model was proportional to the height, confirming the validity of using static pressure data from the model to infer the prototype's differential pressure. Khanal and Lei (2012) proposed a vertical solar chimney with an inclined passive wall plate, and through smoke flow visualization experiments, they observed that the intensity of the return flow at the top of the device was less, the settling depth of the return flow was shallower, and the ventilation efficiency was higher than that of the solar vertical collector with a vertical transparent outer plate. On this basis, Khanal and Lei (2014) also investigated the effect of the tilt angle of the inclined passive plate on the heat flux over the thermal storage layer of the device. The results showed that with the increase of the inclination angle of the outer plate, the return flow at the exit of the chimney gradually decreases, and the airflow rate of the device first rises and then decreases, and there exists an optimal inclination angle that makes the airflow rate of the device maximum. Jing et al.(2015)

built up a vertical solar chimney test model with 2m height, 1m length, and 0.4m-1.2m width to investigate the airflow rate of the test model under the different conditions of the chimney width and the heat flux. They found that the airflow velocity in the runner is directly proportional to the heat flux，and found that the optimal width of the chimney in the range of 0.4m-1.2m is 1m. Zhou et al.(2016) developed a vertical solar chimney power generation test system relying on a high-rise building, and the test data showed that the temperature rise in the system's runner was about 8.13°C, and the maximum air velocity occurred at the top of the chimney, reaching about 0.67 m/s. Rattanongphisat et al. (2017) constructed a square steel chimney with a height of 3 m, inlet/outlet dimensions of 0.4 m×0.4m, square steel plate chimney with a thickness of 1 mm and one side was blackened to collect flow velocity and temperature data in the runner for outdoor tests. The results showed that the airflow velocity near the chimney's blackened surface reached 0.26 m/s Furthermore, the air temperature inside the runner decreased with increasing distance from the blackened surface, with a maximum temperature difference of up to 7°C at the same height, while the temperature difference in the perpendicular direction was only 1.4°C. Bouchair (2022) developed a steady-state heat transfer model for an isothermal vertical chimney. The results shows that if the ambient air temperature depends on the altitude, the results show that the altitude has a significant effect on the thermal performance of the solar chimney. The mass flow rate and heat transfer coefficient increased with increasing chimney height while the air temperature of the chimney decreased with altitude. The optimum width of the chimney decreases slightly. Bagheri and Hassanabad (2023) proposed a SCPP system that can be installed on buildings, and a 1:50 scale model was prepared for experiments using the Energy Ministry of Iran as the study subject. The results showed that the airflow velocity is directly proportional to the height of the chimney and that the operation of the system is affected by temperature and radiation so that higher power can be obtained in summer.

The experimental studies on vertical solar chimneys summarized above have fully investigated the effects of heat flux, device height, runner depth, outer plate inclination, and altitude on the temperature and flow rate of the airflow in the runner and have proposed some measures to strengthen the device's heat storage and heating efficiency. Building upon these successful tests, this paper breaks through by combining solar chimneys with municipal street light, proposing an innovative technological solution to mitigate air pollution in urban street canyons. Our approach leverages the advantages of solar chimney technology in preventing and controlling urban haze and includes in-

depth experimental analysis of filtering materials and airflow characteristics. The experiments confirm the feasibility of integrating solar chimney haze technology with municipal street light for urban dust haze removal, highlighting the effective interaction between solar chimneys and municipal facilities. This provides a solid experimental basis for future research on urban dust haze removal and vertical solar chimneys. Existing methods like the cold-water spraying technique proposed by Lodhi. (1999) require a complex water circulation system and significant water resources, while the solar-assisted large-scale cleaning system (SALSCS) by Cao et al. (2015), despite achieving an air filtration flow rate of 2.64×10^5 m^3/s, is impractical for large-scale application due to its complexity and large footprint. Additionally, the filter-equipped solar chimney power plant by Hachicha et al. (2023), which cleans air by adding filters to both sides of the collector and chimney, incurs high construction and maintenance costs despite its rapid air cleaning capabilities. In contrast, our proposed device is more compact and convenient, enabling more efficient experimentation and data collection, and facilitating modifications for further research. This practical application value provides a new direction and idea for subsequent research in urban air purification technology. Combining the vertical solar chimney technology with the urban street light of the municipal facilities and adding dust removal and purification devices to it, a novel solar chimney dust and haze removal street light integrating the functions of illumination and purification is proposed. The dust removal function of the device operates solely on solar energy conversion, requiring no additional power input. In addition, due to the design incorporating an unpowered wind supercharged wheel, the device can maintain a certain level of dust haze removal through ambient wind at night or in sunless conditions. The haze removal street light not only retains the advantages of solar chimney all-day operation, environmental friendliness, easy maintenance and long life, but also does not change the original urban planning, avoiding urban land occupation, realizing the continuous autonomous purification of vehicular traffic emissions without additional energy input, improving the air quality in the street canyon. As the street light is an important feature of the urban street canyon, it only needs to increase the solar chimney structure and purification device on the basis of the original street light to realize the distributed dust and haze removal function in the street canyon, which has a broad application prospect. This innovative design provides a new strategy with practical application value for solving the urban haze problem, expands the application field of solar chimney technology, and has important theoretical and practical significance. The purpose of the experimental test research in this paper is to

confirm the feasibility of the proposed novel street light device to realize the distributed dust haze in the street and the preliminary understanding of the device operation characteristics, to provide some valuable data support for the subsequent theoretical research and practical design.

1. Test Prototype and Test Device

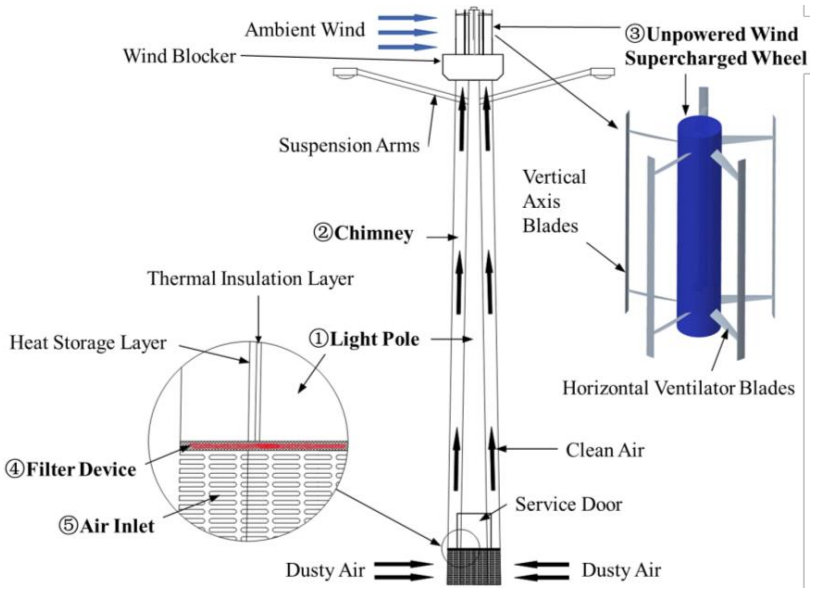

Fig. 1. Test prototype.

The structure and principle of the solar chimney dust haze removal street light proposed in this paper is shown in Fig. 1. The structure of the system device mainly consists of five parts: ①street light body (i.e. light pole), ②vertical solar chimney, ③ unpowered wind supercharged wheel, ④purification filtration device and ⑤air inlet. Around the surface of the light pole, the thermal insulation layer and the heat storage layer are laid in turn. And the heat storage layer at a certain distance and then surrounded by a circular transparent chimney collector, constituting a ring-shaped vertical solar chimney, i.e., airflow, but also the solar chimney collector area. The insulation layer can well isolate the external high temperature heat storage layer to the light pole internal transfer, to protect the original light pole inside the power facilities. The chimney heat collector outside the light pole is made of transparent material, which allows maximum sunlight transmission to the internal heat storage layer while minimizing its own reflection. The suspension arms extend from the same-sized window cut into the upper part of the inner wall of the chimney collector, providing support for the main body of the chimney. Regular air inlets were opened at the bottom

of the inner wall of the chimney collector. In accordance with the results of the Zuo et al. (2022) the height of the air inlet is set between 0~0.6m to realize the efficient capture of the highest PM_{10} concentration zone generated by the traffic emissions. The purification filtration unit was horizontally mounted at the top of the air inlet, located at the bottom of the chimney cowl. This unit efficiently purifies the dusty, haze-containing airflow, ensuring the cleanliness of the chimney's interior flow path above. Additionally, it reduces the impact of sunlight shading caused by dusty haze particles within the flow path. At the top is an unpowered wind supercharged wheel innovatively designed by Zuo et al. (2018), which consists of a rigid combination of vertical axis wind turbine blades and pairs of upper and lower horizontal ventilator runner blades used to enhance the pumping force in the chimney flow path. Purifications that have reached the end of their service life are replaced through a service door on the chimney inner wall.

Solar chimney dust haze removal street light dust haze removal works as follows: As the sun rises, the transparent chimney heat collector cover allows the sun's direct and scattered radiation pass through, and most of this radiation is absorbed and stored by the heat storage layer and warms up. At the same time, the transparent collector will impede the long-wave radiation emitted from the surface of the heat storage layer, thus increasing the air temperature and decreasing the density in the circular chimney runner inside the cover, thus increasing the air temperature and decreasing the density in the circular chimney runner inside the cover, forming the greenhouse effect. Under the greenhouse effect, the air in the chimney runner and the ambient cold air outside the chimney form an internal and external pressure difference, i.e., the thermal pressure and float, forming an upward-flowing airflow. The chimney effect can increase the pumping force in the chimney runners, which in turn enhances the upward flow of airflow along the chimney runners. Therefore, under the action of solar chimney pumping force, the surrounding cold dusty air will be continuously sucked into the chimney runner from the air inlet at the bottom of the street light. The air then flows upward along the chimney runner. As it passes through the clean filtration device located at the upper part of the air inlet, PM_{10} particles are intercepted by the filtration device, effectively purifying the dust and haze, turn into clean air. Clean airflow along the chimney heat collection area is heated while flowing upward, and then finally discharged from the top of the chimney, so as to complete an environmental dust haze cold air purification cycle.

The high-altitude ambient wind will drive the vertical axis blades of the wind

supercharged wheel to rotate, thus driving the horizontal ventilator blades to rotate, generating negative pressure at the bottom of the wind supercharged wheel, i.e., at the

Fig. 2. Experimental Model.

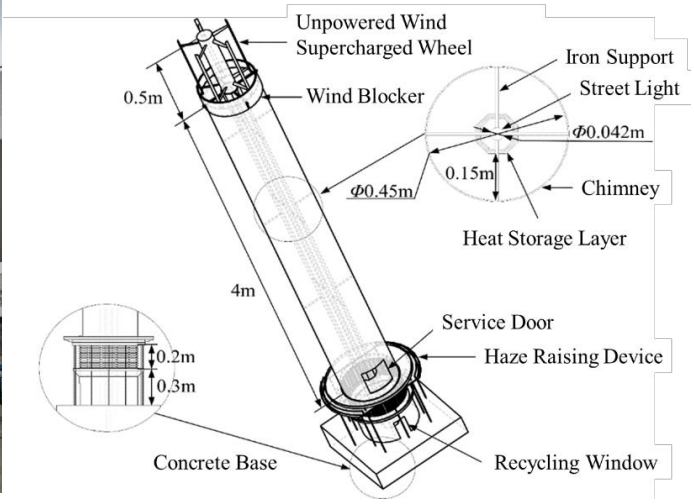

Fig. 3. Model Geometric Dimensions.

exit of the top of the annular chimney, further increasing the suction effect of the chimney runner, and enhancing the upward flow of the airflow.

Fig. 2 shows a photograph of a mini solar chimney dust haze removal street light experimental model, while Fig. 3 illustrates its geometric dimensions.. The experiment site was conducted on the roof of Qinxue Building, Jiangning Campus, Hohai University, China. The test setup mainly consists of six parts: street light pole, chimney body, unpowered wind supercharged wheel, wind blocker, purification and haze raising device:

(1) The street light pole is a seamless steel pipe with a length of 4,000mm, a diameter of 42mm and a thickness of 4mm, with a thermal insulation layer laid on the surface.

(2) The chimney body: the heat storage layer is made of 15mm thick wooden plywood, laminated to the outer wall of the street light pole, which is in the shape of an external octagon with a diameter of 114mm, and the outer surface is coated with black in order to improve the absorption rate of solar irradiance. A gap between the heat storage layer and the street light pole accommodates test and measurement instruments cables, while the remaining space is filled with asbestos to prevent heat transfer from the heat storage layer to the interior. This ensures that the pigtail line is in a normal operating temperature environment. The chimney collector is made of 4mm thick endurance sheet rolled into a cylinder. The main body of the chimney collector is 4000mm high, 450mm in diameter, and the circular air runner is 150mm wide.

(3) Unpowered wind supercharged wheel: height 500mm, impeller diameter 450mm, its ventilator runner blade made of iron, choose CLARK Y wing type; vertical axis blade made of PVC, choose NACA 0012 wing type.

(4) Wind blocker: located in the wind supercharged wheel and chimney outlet of the connection, 100mm high, 460mm in diameter, 10mm in thickness, the material is transparent plexiglass. Its role is equivalent to the extension of the chimney runner, so that the wind supercharged wheel of the lower side of the ventilator rotor as much as possible to suck the airflow in the chimney runner, to enhance the negative pressure effect produced by the wind supercharged wheel.

(5) Purification: consists of a cross bracket and two half-ring filters, the inner ring is octagonal, 114mm in diameter; the outer ring is circular, 450mm in diameter. The two half-ring filters are docked and placed on the bracket, constituting a whole ring of filtration clean device. The inner and outer edges of the purification is sealed with the combination of heat storage layer and endurance plate cover respectively to ensure that the chimney gas flow passes through the runner purification.

(6) Haze raising device: in the chimney inlet outside the construction of a simple haze raising device, the principle of its operation is hourglass method, where air-dried, finely ground sand trickles down evenly from an upper annular funnel, hitting a lower small funnel and the chimney base, raising a large amount of dust. The height of the air inlet of the test model was 0.3 m to 0.5 m. It was found in the experiment that it was not possible to realize the continuous fall of the sand by its own weight alone, so the work of haze raising in the experiment was still completed by manual assistance. This involved frequently tapping the edges of the funnel by hand to use vibrations to help the sand fall.

2. Test Data Acquisition System

Fig. 4. Ambient measuring pole.

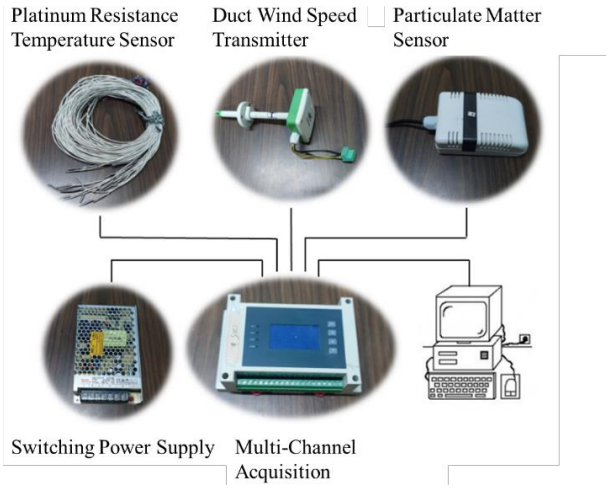

Fig. 5. Measuring sensors.

In the operation performance test of solar chimney dust haze removal street light, the test parameters to be measured are solar irradiance, ambient temperature and humidity, ambient wind speed, chimney runner airflow rate and temperature, temperature of the heat storage layer, chimney collector surface temperature and haze concentration before and after the purification, etc., which are all collected by the automatic measurement and acquisition system. The measuring instruments were arranged on an ambient measuring pole 3 m away from the test setup, as shown in Fig. 4. Fig. 5 illustrates the measurement sensors used in the test to collect the temperature、flow rate、the temperature of the heat storage layer and the haze concentration at each temperature measurement point in the chimney runner. Since the temperatures of the airflow and the heat storage layer in the model remain low, not exceeding 100°C, platinum resistance temperature sensors with high accuracy for low-temperature measurement were selected. The relevant parameters of each sensor are summarized in Table 1.

Table 1

Table of summary of various sensors.

Instrument	Model	Range	Accuracy, error
Total solar radiation sensor	RS-RA-*-JT	0~1800 W/m^2	1 W/m^2, ±2%
Temperature and humidity sensor	RS-WS-N01-SMG	−40 ℃~+120 ℃，0% RH~80% RH	±3% RH，±0.5℃, (25 ℃)
Three-cup wind speed sensor	RS-FSJT-*	0~30 m/s	±(0.2+0.03V) m/s
Temperature sensor	WZP-PT100	−40 ℃~+200 ℃	±(0.15+0.002T) ℃

Duct wind speed transmitter	RS-FS-*-9TH	0~15 m/s	±(0.2+2%FS) m/s
Particulate matter sensor	JXBS-3001-PM	0-1000 μg/m^3	±(10%PM) μg/m^3

The acquisition system and measurement point arrangement in the solar chimney dust haze removal street light test model are depicted in Fig. 6. Along the vertical chimney runner, a total of five temperature measurement point systems were arranged, labeled ①~⑤ according to the direction of airflow from bottom to top. Each temperature measurement point system on the horizontal layer includes measurements for the surface temperature of the heat storage layer, the airflow temperature, and the temperature of the inner surface of collector. Except for the temperature measurement point system ⑤ at the chimney outlet, all other neighboring measurement point systems maintain a height difference of 1m. Additionally, three airflow rate and three dust concentration measurement points were also set up in the experiment, which were arranged in pairs at the inlet, middle and outlet of the chimney. All sensor output signals were converted to digital signals and connected to an RS485 communication bus. Connected to the monitoring computer via an RS485 to USB converter, the measured data were recorded with the help of a real-time data acquisition system composed of self-developed solar chimney integrated system performance testing software with Windows XP as the operating system. During this test, the automatic data acquisition interval was set to 1 minute.

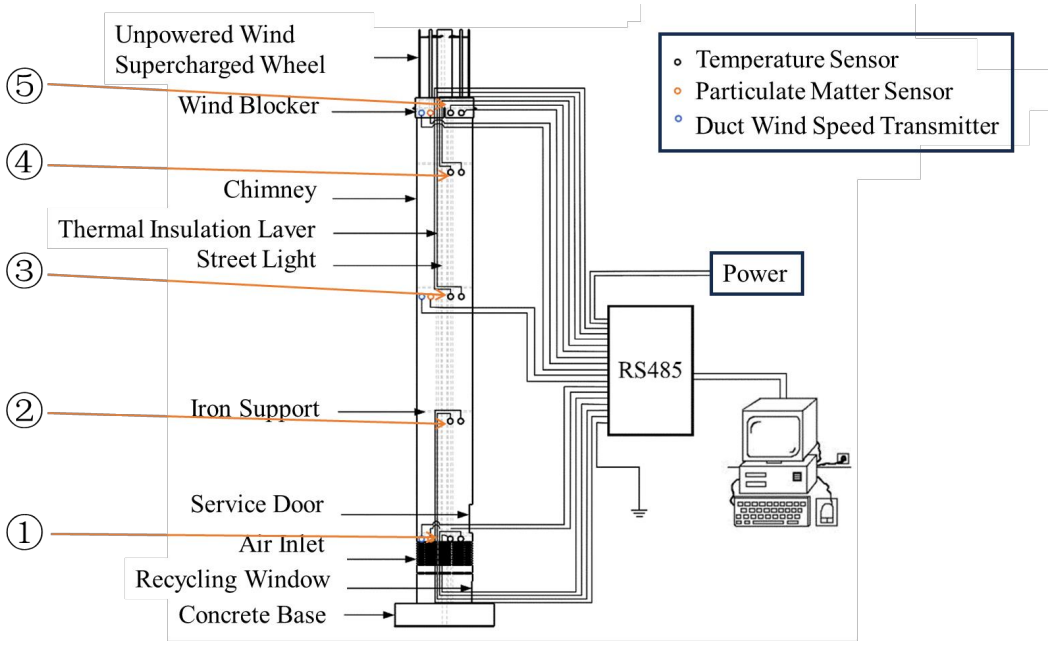

Fig. 6. Acquisition system and measurement point arrangement of the experiment.

3. Uncertainty Analysis of Experimental Results.

To evaluate the accuracy of the experimental data, the collected data need an uncertainty analysis. Measurement uncertainty is usually regarded as the standard deviation of the probability distribution of the state of knowledge over the values that correspond to the values that may be measured. The relative uncertainty is the measurement uncertainty relative to the magnitude of a particular selection of values (that selected value is non-zero). Often this selection is referred to as the measured value. According to the nature of the errors and their causes, the errors can be classified into three categories: random errors, systematic errors, and personal errors. Before the experiment was carried out, all the measuring instruments had been calibrated, and each clean filtration scheme was optimized to the best of our ability, thus systematic errors can be considered negligible. As the data in this experiment were collected by the automatic measurement acquisition system, personal errors are not a concern. Random error is the statistical fluctuation in the measurement data due to the precision limitation of the measuring instrument, although it cannot be avoided, the method of probability statistics can be used to reduce the random error to improve the precision of the experimental data. The following statistical analysis is used to estimate the random error:

The arithmetic mean of N data is:

$$\bar{x} = \frac{1}{N}\sum_{i=1}^{N} x_i \tag{1}$$

Then the standard deviation is:

$$\sigma = \sqrt{\frac{1}{N-1}\sum_{i=1}^{N}\left(x_i - \bar{x}\right)^2} \tag{2}$$

And the standard error of the mean is:

$$S = \frac{\sigma}{\sqrt{N-1}} \tag{3}$$

All the parameters measured in this paper are direct measurements, including ambient temperature, ambient humidity, solar irradiance, ambient wind speed, temperature of Pt100, airflow rate, and dust concentration. Relative uncertainty or relative error is calculated as the ratio of the uncertainty of a measurement to the size of the measurement, given by the formula: Relative uncertainty= Absolute uncertainty/ measured value (Helmenstine, A.M., 2015).

The experimental data from 6.00 to 18.00 on September 16, 2021 were selected to

make an error analysis of the parameters such as ambient temperature, humidity and solar irradiance, as well as chimney runner air temperature, wind speed, heat storage layer temperature, chimney collector inner surface temperature and dust concentration at each measurement point in the experiment, and the results of the error analysis are shown in Table 2.

Table 2

Table of results of error analysis of experimental data.

Parameter	Standard error	Relative Uncertainty
Ambient temperature	±0.0789 ℃	0.3849%
Ambient humidity	±0.339	0.867%
Solar Irradiance	±8.909 W/m^2	3.639%
Ambient wind speed	±0.0147 m/s	7.368%
Temperature of Pt100	±0.337 ℃	1.453%
Airflow rate	±0.0136 m/s	6.816%
Dust concentration	±0.157 μg/m^3	4.361%

One reason for the large relative uncertainty of the ambient wind speed and airflow rate may be that the precision of the instrument for measuring wind speed is not high enough, especially at low wind speeds (i.e., wind speeds of ≤0.1 m/s). Additionally, the wind speed instability, caused by the circuit's principles, might result in the measurement instrument's data not being stable when the device automatically records the data.

4. Test Results and Discussions

4.1. Meteorological Condition

The no-load test of the flow field characteristics of the test model was conducted on September 16th-17th.

Fig. 7 shows the variation curves of solar irradiance, ambient temperature, and humidity on the test days. The sunrise and sunset times on the test day were around 6:00 and 18:00, respectively. On the 16th, the solar radiation showed an oscillating sinusoidal distribution. Under the influence of cloud cover, the solar irradiance oscillated up and down frequently at noon, and reached a maximum of 1027.2 W/m^2 at 12:30, with an average irradiance of 551.9 W/m^2 from sunrise to sunset. The solar radiation on the 17th also followed a sinusoidal distribution, with a maximum irradiance of 936 W/m^2 at about 12:00. After that, the solar irradiance appeared to oscillate up and down with slight frequency under the influence of cloud cover until about 15:00, and the average irradiance from sunrise to sunset was 535.5 W/m^2.

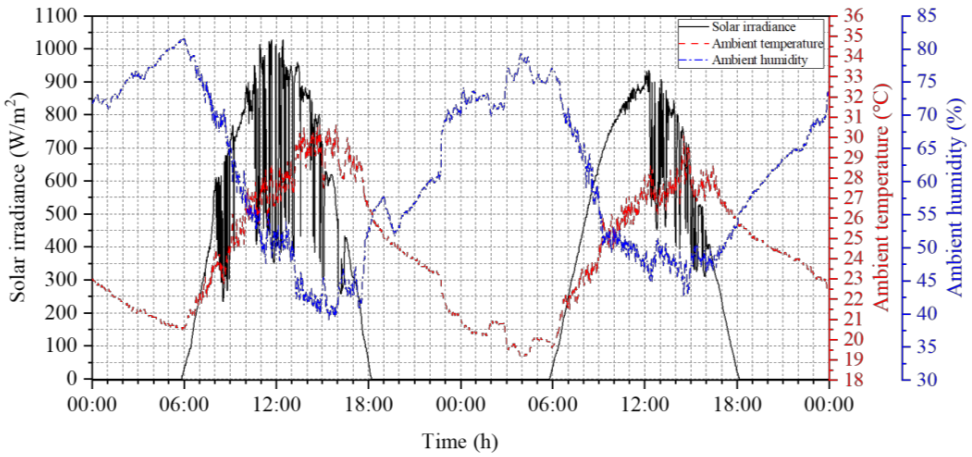

Fig. 7. Solar radiation intensity, ambient temperature and humidity daily variation curves.

The ambient temperature curve exhibits a pattern similar to that of the solar irradiance, albeit with an obvious lag in temperature peak compared to the irradiance peak. On the 16th, the temperature peaked around 16:00 at 30.6℃, while it reached its lowest point around 6:00 at 20.5℃, resulting in an average temperature of 24.7℃, and the difference in temperature between day and night was 10.1℃. Similarly, on the17th, the temperature peaked around 14:30 at 30.1℃, and reached its lowest point around 4:00 at 19.2℃, with the difference in temperature between day and night being 10.9℃. the average temperature was 24.0°C, and the temperature difference between day and night was 10.9°C. The ambient humidity variation curve was highly negatively correlated with the ambient temperature variation curve. When the ambient temperature was the lowest, the ambient humidity reached its the highest, and vice versa. The maximum daily relative humidity in the 16th and 17th days is about 81.6% and 77.4%, respectively, and the minimum daily relative humidity is 40.3% and 45.7%, respectively.

The above results indicate that the test day belongs to the typical meteorological characteristics of late summer cloudy days and is representative of late summer cloudy weather.

4.2. Analysis of No-load Flow Field Characteristics

In order to investigate the flow field characteristics in the air runner of the solar chimney dust haze removal street light, the test was carried out for the no-load condition, i.e., the condition with no purification installed.

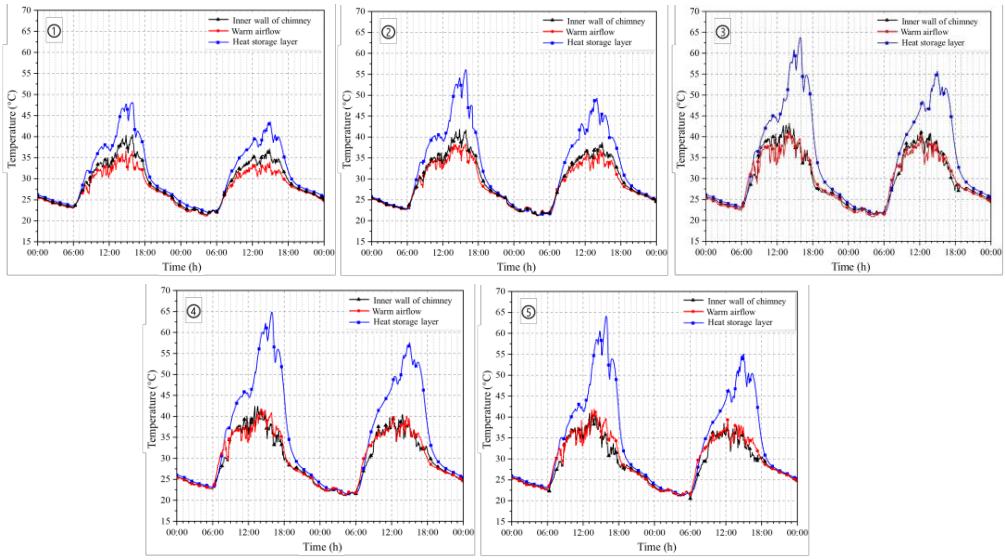

(a). Daily variation curves of the temperature of the inner wall of the chimney, the airflow and the heat storage layer for the same point system.

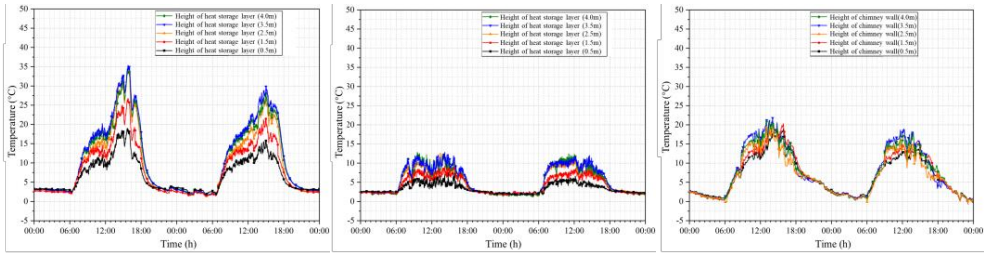

(b). Daily variation curves of collector wall, airflow and heat storage layer temperatures for different point systems.

Fig. 8. Daily variation curve of the temperature of the experimental device.

Fig. 8 shows the daily variation curves of temperature for the five measurement point systems in the solar chimney dust haze removal street light test model. Fig. 9 shows the temperature distribution curves from the bottom to the top of the chimney of the solar chimney dust haze removal street light test model at different time layers every 3 hours. As can be seen from Fig. 8(a) and (b), it is evident that the temperature trends of the five point systems in the test model follow a sinusoidal function. However, in each point system, the peak time of the temperature at each point is not consistent. The temperatures of the inner wall of the chimney collector and the airflow peaked first, and the temperature of the heat storage layer reached the peak with a lag. On the 16th day, the heat storage layer temperatures peaked around 16:00 in each point system, and the temperatures of the airflow in the flow path and the inner wall of the collector peaked around 14:00. The peak heat storage layer temperatures were much higher than the peak temperatures of the collector walls and airflow, and overall, the heat storage layer temperatures were much higher than the temperatures of the collector walls and airflow in the runners.

This is because the heat storage role of wood plywood has a large specific heat capacity of 2512 J /(kg·K), its thermal inertia is larger; while the heat collector of the material of the specific heat capacity of the endurance plate and the specific heat capacity of the air to be smaller, respectively, 1170 J/(kg·K) and 1005 J/(kg·K), so the unit area of absorption of the same solar radiation, the heat storage layer warming slower than the collector wall and the air flow rate of warming, the peak temperature of the storage layer lags behind. After sunrise, most of the solar radiation energy through the transparent chimney collector wall, blackened heat storage layer is absorbed and converted into heat energy, characterized as temperature rise. The high heat capacity and thermal energy storage capacity of the wood plywood heat storage layer makes the temperature of the heat storage layer much larger than that of the inner wall of the collector and the airflow, and the temperature peak is also much larger than that of the inner wall of the collector and the airflow. Fig. 8 also shows that, during the sunrise to sunset, the collector wall and airflow temperature change oscillation frequency is significantly greater than the heat storage layer temperature change oscillation frequency, these phenomena indicate that in the high solar irradiance during the chimney collector wall and airflow heat exchange is intense, the direction of heat exchange is not certain, while the heat storage layer is stable to the airflow of heat supply, wood plywood heat storage layer has a good heat storage function.

The temperature distribution along the chimney height direction of the airflow is analyzed, it can be seen from Fig. 8(b) and Fig. 9 that the temperatures of the inner wall of the collector, the airflow and the heat storage layer all increase and then decrease with the increase of the chimney height, and reach the peak value in the measurement point system of ④, which is at a height of 3.5m. However, the temperature data obtained at the measurement point system ⑤ decrease due to the presence of a wind blocker installed at the top of the chimney. This blocker partially obstructs the end region of the heat storage layer at a height of 4 m, consequently lowering the temperature at each measurement point of point system ⑤.

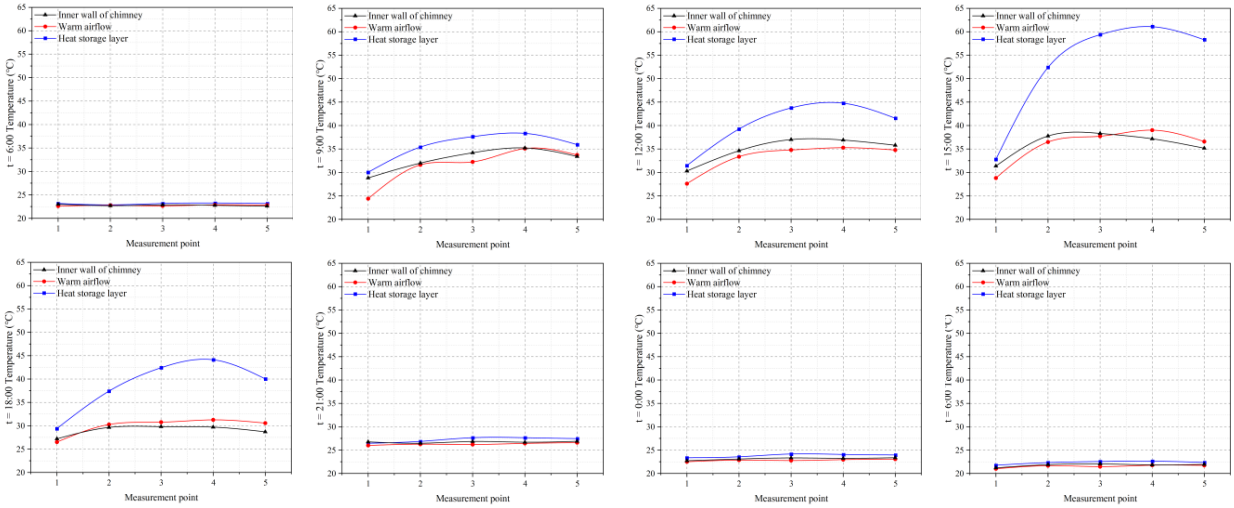

Fig. 9. Temperature distribution curve from the bottom to the top of the chimney of the test model.

There are differences in the rate of warming between the point systems, with the points below point ③, at a height of 2.5 m, warming rapidly while those above point 3 warming slowly. As the air flows upward along the runner, the greatest warming occurs when the air flows from measurement point system ① to measurement point system ②, and there is a significant cooling when the air flows from measurement point system ④ to measurement point system ⑤. This disparity arises because the ambient cold air just entered the chimney heat col-lection area, with a low temperature and minimal temperature difference compared to the surroundings. So very little heat is lost through convection to the environment. Meanwhile, the temperature difference between the air and the collector wall, as well as the heat storage layer, is considerable, leading to substantial heat absorption from their surfaces. The phenomenon manifests as the maximum warming amplitude, showing that the bulk of heat absorption and exchange occurs primarily in this region. In the near vicinity of the measuring point system ⑤ of the test device, the shading influence of the wind blocker makes the temperature of the inner wall of the collector and the heat storage layer start to decrease. The temperature difference between the hot airflow and the heat storage layer decreases, and the absorbed heat becomes less, and there are periods of time when the temperature of the inner wall of the collector hood starts to be lower than that of the hot airflow, and the air on the near-wall side starts to dissipate the heat transfer through the convection of the collector hood to the outside, resulting in the temperature falling back, and there is a significant temperature drop.

The maximum temperatures in the heat storage layer on the 16th and 17th were 64.8°C and 57.1°C, the minimum temperatures were 23.2°C and 21.9°C, and the daily maximum temperature rise was 41.6°C and 35.2°C, respectively; the maximum

temperatures in the inner wall of the collector were 42.4°C and 40.5°C, the minimum temperatures were 22.9°C and 21.2°C, and the daily maximum temperature rise was 19.5°C and 19.3°C, respectively. The air maximum temperatures in the runner were 41.8°C and 40.1°C, the minimum temperatures were 22.8°C and 21.2°C, and the daily maximum temperature rise was 19.0°C and 18.9°C, respectively. The minimum temperature at each measurement point of the heat storage layer was 1~2°C higher than the ambient minimum temperature. This is precisely because the heat storage layer is covered by the outer collector, the air in the runner has become a temporary "insulation layer" of the heat storage layer, which makes the temperature of the heat storage layer fall slower than the ambient temperature.

It can also be seen in Fig. 8 and Fig. 9 that between 13:00 and 19:00, the temperature of the air above the measurement point system ① is higher than the temperature of the inner wall of the collector. Due to the heat storage layer's thermal lag and large heat storage capacity, the heat storage layer temperature during this time is the highest of the day and is much higher than the airflow and chimney inner wall temperatures. By the immediate vicinity of the high-temperature heat storage layer, the airflow heating rate exceeds the chimney wall heating rate, the air temperature is higher than the temperature of the inner wall, and then reverse heating chimney wall, through the chimney wall outward heat transfer, the loss of heat carried. This heat transfer phenomenon leads to the further heating of the hot airflow is blocked, the heating curve becomes flat, and even in the chimney outlet area there is a tendency for the temperature to drop. Reflux occurs when the temperature of the hot airflow exiting the top of the stack is lower than the temperature of the airflow below it. The backflow phenomenon can significantly hinder the suction in the flow path of the test unit, so in the subsequent optimization design of the structure, it is necessary to fully consider how to attenuate the chimney backflow phenomenon.

Fig. 10 shows the daily variation curves of airflow rate in the chimney runner of the solar chimney dust haze removal street light test model. The daily variation curves exhibit a sinusoidal function, closely mirroring the trend of air temperature change. On the 16th, the maximum flow rate of the airflow in the runner with a height of only 4m was measured around 11:00, reaching 1.8m/s, and the average flow rate of the whole day was 0.53m/s. The maximum flow rate of the airflow in the runner was also measured on the 17th at around 11:00, reaching 1.7m/s, and the average flow rate of the whole day was 0.41m/s. The above data can show that the solar chimney dust haze removal street light test model creates an upward hot airflow despite the device chimney

height is only 4m. It is worth noting that the airflow with an average flow rate of 0.36m/s and a maximum instantaneous flow rate of 1.3m/s occurred paradoxically in the chimney from about 0:00am to 1:30am on the morning of the 16th, while the same phenomenon did not occur in the early morning of the 17th in comparison. Comparing the ambient wind conditions of the two days, it can be seen that the early morning of the 16th was windy with an average wind speed of 1.2m/s, while the early morning of the 17th was basically windless, which shows that the ambient wind speed at night played a positive role in the airflow buoyancy inside the chimney, whereas the ambient wind will accelerate convective heat dissipation from the chimney wall after sunrise, and the total effect needs to be further investigated.

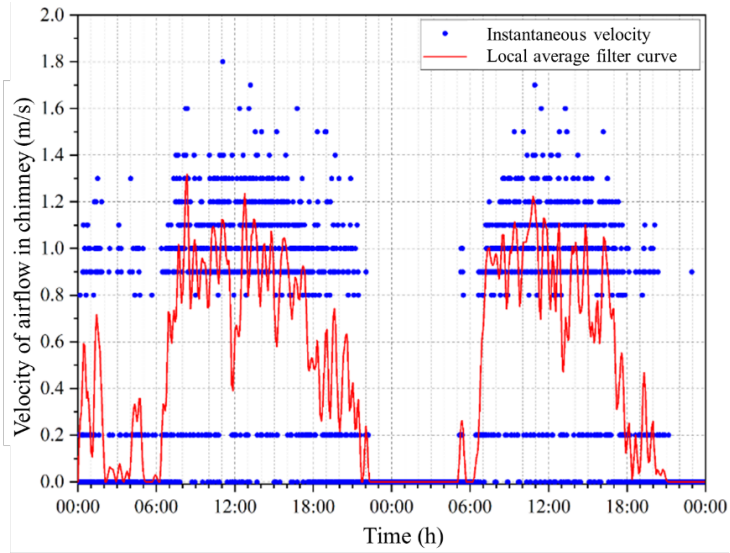

Fig. 10. Daily variation curve of airflow rate in chimney runner.

The solar dust haze chimney heat collection efficiency η_C is calculated as:

$$\eta_C = Q / A_C G \tag{4}$$

Where G is the solar irradiance received by the solar dust haze chimney, W/m². Q is the useful heat gained by the solar chimney collector hood, W.

Q is calculated as:

$$Q = m c_f \Delta T \tag{5}$$

Where m is the mass flow rate of the airflow in the solar dust haze chimney, kg/s. c_f is the specific heat capacity of the airflow. ΔT is the temperature rise of the airflow in

the chimney, ℃.

The average heat collection efficiency of the solar haze chimney was calculated to be 42.64% and 31.63% on the 16th and 17th, respectively.

4.3. Test and Analysis of Different Clean Filtration Schemes

The purification filtration device is the core part of solar chimney dust haze removal street light, and the filtration layer will inevitably create pressure drop inside the chimney, hindering the rise of hot airflow. Therefore, it is crucial to choose a suitable purification for solar chimney dust haze removal street light, and balance the filtration efficiency of the filter material and the pressure drop it brings.

In this paper, several common filter materials on the market, including HEPA, primary filter cotton, activated carbon, nylon filter screen and so on, are used as the main test objects. Fig. 11 shows these filter materials, which have been cut to fit the chimney collector runners. The thickness of HEPA, primary filter cotton and activated carbon is 10mm a layer, while the thickness of nylon filter screen is 2mm a layer, in order to increase the number of layers of filter materials to test the filtration effect under different filter material thicknesses. The various clean filtration schemes in the experiment are shown in Table 3.

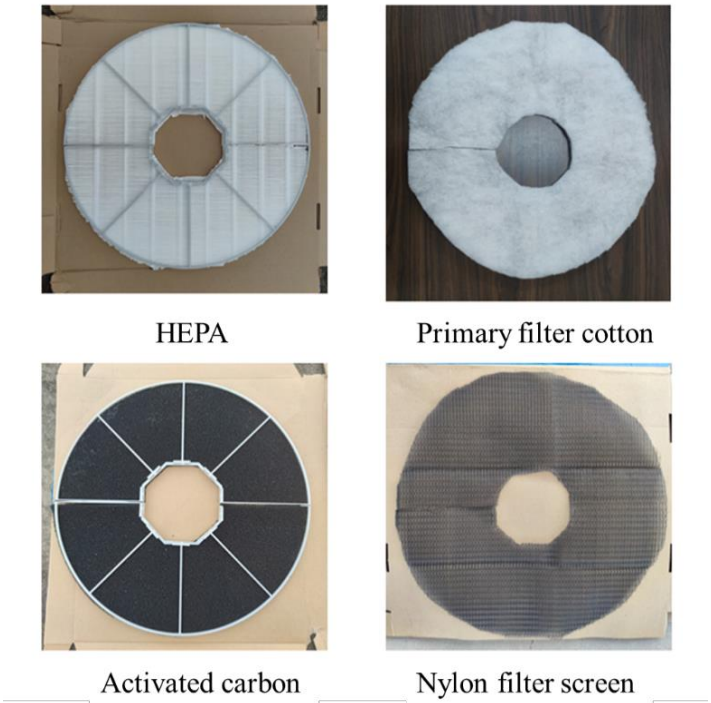

Fig. 11. Filter materials.

Table 3

Table of different filtration schemes (√ for one layer of this filter material).

Experiment number	HEPA	Primary filter cotton	Activated Carbon	Nylon Filter Screen
C1	√			
C2		√		
C3		√ √		
C4			√	
C5			√ √	
C6				√
C7				√ √
C8				√ √ √
C9				√ √ √ √
C10				√ √ √ √ √
C11		√		√
C12			√	√
C13			√ √	√

The filtration experiments were conducted from September 18 to September 24, all under sunny conditions, with average daily temperatures of 25.6°C, 28.6°C, 26.8°C, 27.3°C, 27.4°C, 25.9°C, and 26.1°C, respectively. Since the test device is small, only 4 m in height, and the runner suction power that can be obtained is far less than the that obtained from a street light of the same height as an actual utility pole of 12 m, it is chosen in each experimental day to start the purification and filtration experiments when the maximum temperature of the heat storage layer reaches 60 ℃, which is around 14:00, and to end the experiments when the temperature of the heat storage layer falls to below 40 ℃, which is around 17:00. Data collection occurred automatically every minute, with each filtration condition being tested for a duration of 30 minutes.

In the experimental data obtained, the average filtration efficiency $\overline{\mu}$ of each filter screen can be expressed as:

$$\overline{\mu} = \frac{\sum_{i=1}^{n} \mu(i)}{n} \tag{6}$$

Where n is the number of data collected in each filtration condition and has a value of 30; $\mu(i)$ is the instantaneous filtration efficiency of the filter screen, which can be expressed as:

$$\mu(i) = \frac{c_{before}(i) - c_{after}(i) - \alpha + \beta}{c_{before}(i) - \alpha} \tag{7}$$

Where $c_{before}(i)$ and $c_{after}(i)$ are the dust concentration before and after the filter screen at the moment t after dust raising, respectively; α and β are the average

dust concentration before and after the purification in the initial environment, respectively.

To scientifically show the pressure, drop effect of each filtration scheme, the experimental data with relatively small cloud shading effect in the no-load flow field characterization experiments, that is, the airflow rate data in the chimney runner at the corresponding time period in the middle of the 17th day, is selected to act as the reference for each clean filtration condition. The total internal and external pressure difference Δp of the vertical solar chimney is (Li, 2011):

$$\Delta p_h = \frac{1}{2}\rho_0 g H \frac{\Delta T}{T_0} \tag{8}$$

Where ρ_0 is the ambient air density; g is the local gravitational acceleration with a value of 9.81 m/s^2; H is the height of the vertical heat-collecting area; ΔT is the air temperature difference between the chimney inlet and outlet; and T_0 is the ambient temperature. In turn, the pressure drop of the various purifications is:

$$\Delta P = \Delta p_{load} - \Delta p_{black} \tag{9}$$

Where Δp_{load} and Δp_{black} are the pressure difference between the test setup under no-load and real-load conditions, respectively.

By calculating the clean air mass flow of the filter screen in each clean filtration scheme, the performance of the clean filtration scheme in the solar chimney dust haze removal street light is measured, and this is used as the main basis for selecting the most suitable clean filtration scheme for the solar chimney dust haze removal street light. The clean air mass flow of the filter screen after loading is (Spencer, 2001):

$$m = \frac{\bar{\mu} C_D A [2gH\rho\Delta\rho]^{1/2}}{(1 + A_r^2)^{1/2}} \tag{10}$$

where C_D is the flow coefficient, which takes the value of 0.6 (Spencer, 2001) because the Reynolds number of the hot airflow inside the chimney is much larger than 100; A is the chimney outlet area; $\Delta\rho$ is the chimney internal and external air density difference ; and A_r is the ratio of the chimney outlet area to the inlet area.

Fig. 12 shows the filtration efficiency of single-layer filter screens made of different materials alongside their corresponding variation curves of airflow velocity in the runner. The red dotted line represents the average filtration efficiency, and the blue dotted line represents the average airflow rate. As can be seen from the figure, both curves have an oscillatory distribution with the filtration time, and generally satisfy the

trend of decreasing airflow velocity in the chimney runner when the filtration efficiency increases, and vice versa.

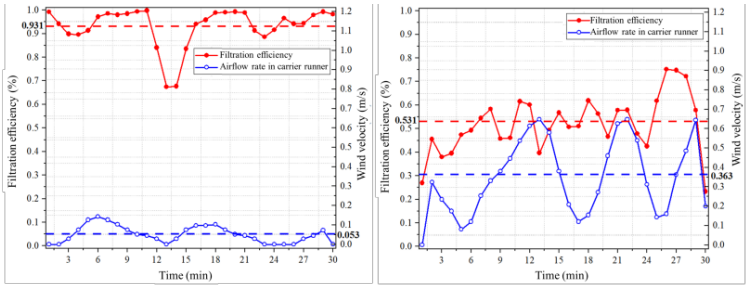

(**C1:** HEPA) (**C2:** Primary filter cotton)

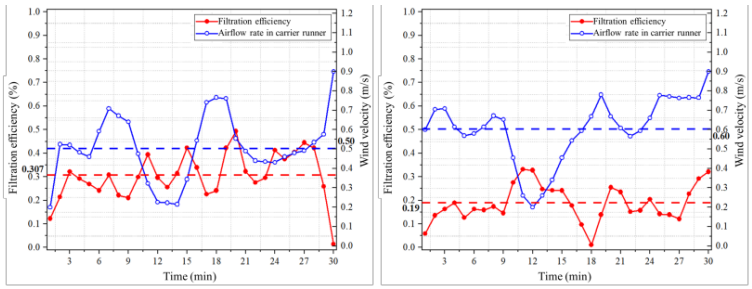

(**C4:** Activated carbon) (**C6:** Nylon filter screen)

Fig. 12. Filtration efficiency of different filter materials and their corresponding airflow rates in the runner.

Comparing C1 (a layer of HEPA), C2 (a layer of primary filter cotton), C4 (a layer of activated carbon) and C6 (a layer of nylon filter screen) in Fig. 12, it can be seen that the filtration efficiency of the four materials filter screen is in the following order: HEPA > primary filter cotton > activated carbon > nylon filter screen. Because HEPA and primary filter cotton are multi-layer fiber structure, offer a larger adsorption surface area, resulting in better filtration performance. However, the pores of primary filter cotton are larger than those of HEPA, so its filtration efficiency is lower than that of HEPA. Although the adsorption surface area of activated carbon is large, but the diameter of its effective adsorption microporous nanoscale, much smaller than the diameter of PM, which is more suitable for the net removal of harmful gases. Furthermore, activated carbon screen pores are larger, the capture rate of PM is significantly lower than the multi-layer fiber structure. Nylon filter screen for single-layer pore structure, adsorption surface area is small, the capture capacity of PM is poor, the lowest filtration efficiency.

The order of airflow rate in the chimney runner is the opposite of the order of filtration efficiency, nylon filter screen > activated carbon > primary filter cotton > HEPA, which indicates that the filtration efficiency of different filter screens is

inversely proportional to their air resistance. Considering the suction capacity of the purification, the selection of the subsequent purification needs to be weighed between the filtration efficiency and its air resistance.

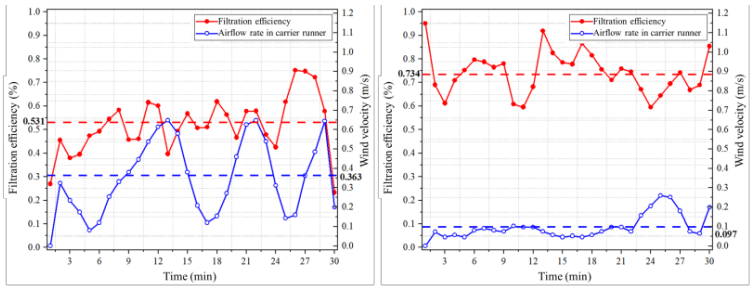

(**C2**：Single layer) (**C3**：Two-layer)

(a). Primary filter cotton.

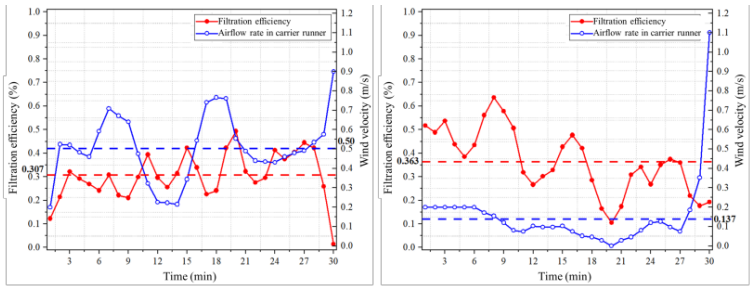

(**C4**：Single layer) (**C5**：Two-layer)

(b). Activated carbon.

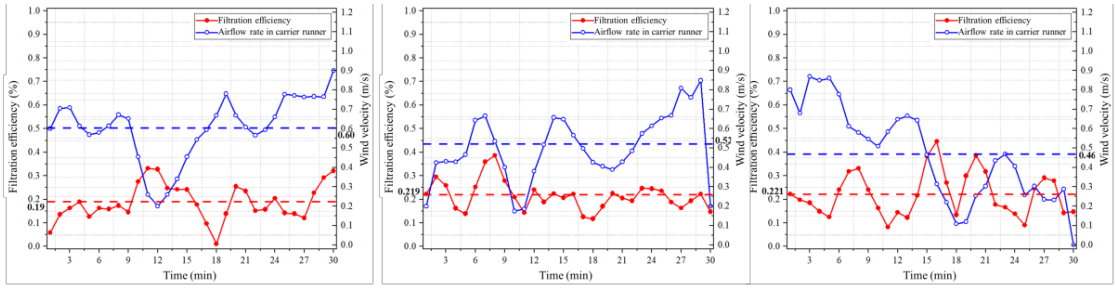

(**C6**：Single layer) (**C7**：Two-layer) (**C8**：Three-layer)

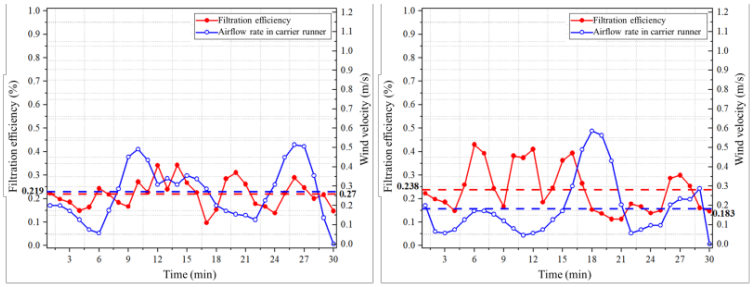

(**C9**：Four-layer) (**C10**：Five-layer)

(c). Nylon filter screen.

Fig. 13. Filtration efficiency of different filter screen thicknesses and their corresponding airflow rates in the runner.

Fig. 13 shows the performance of various material filter screens when loaded with different thicknesses. As can be seen from the figure, the filtration efficiency improved by increasing the thickness of the multi-layer fiber structure filter screen, is higher than that of increasing the thickness of the single-layer fiber structure filter screen. Consequently, multi-layer fiber structure filter screens exhibit higher air resistance, leading to a greater reduction in airflow rate in the runner. This is because the pores of the primary filter cotton are small, and increasing its thickness prolongs the duration of dusty airflow, thereby improving the adsorption efficiency of PM. At the same time, it also improves the overall pressure drop and reduces the airflow rate in the chimney runner. Activated carbon, on the other hand, has the small diameter of the effective adsorption micropore, resulting in weak PM attachment ability. PM adsorbed in the airflow may be re-adsorbed, rendering the increase in thickness of activated carbon screens to enhance filtration efficiency only slightly. Nylon filter screen material surface smooth, and PM weak force, also not easy to adsorb PM, so its filtration efficiency is not sensitive to the thickness. Comparison of C6, C7, C8, C9 and C10 in Fig. 13(c) shows that the increase in the number of layers of the same type of filter screen results in a much smaller increase in filtration efficiency than the decrease in airflow rate in the chimney runner, which is in line with the conclusions drawn in the Liu (2020). Therefore, the 4m high solar chimney dust haze removal street light is not suitable for loading filter screens with higher thickness.

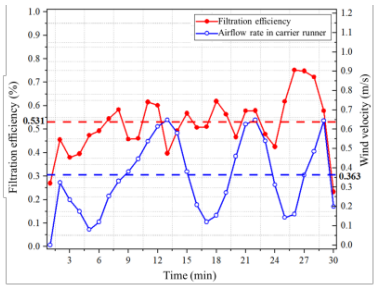

(**C2:** Primary filter cotton)

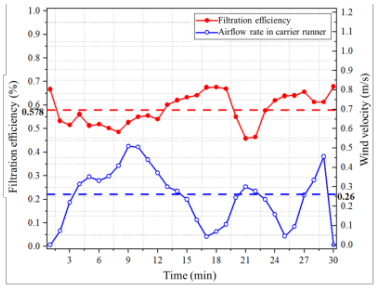

(**C11:** Primary filter screen+ Nylon filter screen)

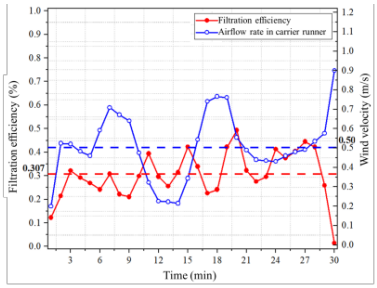

(**C4:** Activated carbon)

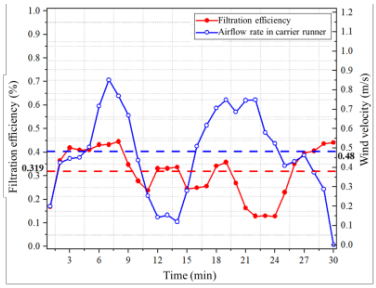

(**C12:** Activated carbon+ Nylon filter screen)

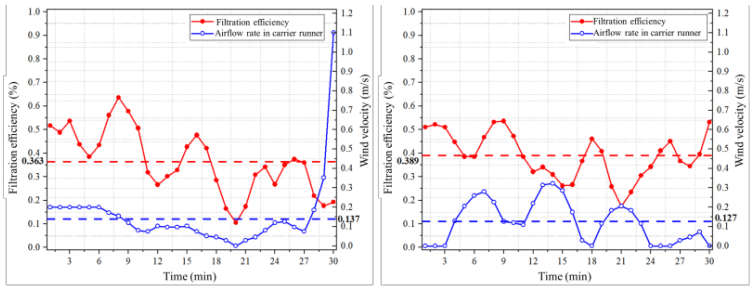

(**C5:** Tow-layer activated carbon)**(C13:** Two-layer activated carbon+ Nylon filter screen)

Fig. 14. Combined filter screen filtration efficiency and its corresponding airflow rate in the runner.

Fig. 14 illustrates the performance of the filter screen under the combination of different materials. When the filter screens of different materials are used in combination, the one that plays the main filtering role is the one with the highest filtration efficiency. Typically, the filtration efficiency of the whole combination of filter screens increases slightly, and the airflow rate in the chimney runner decreases slightly. Initially, the dusty airflow first contacts the first layer of nylon filter screen with larger pores, and the large-sized PM in the airflow is first filtered by the first layer of nylon filter screen, allowing the second layer of main filter screen to mainly adsorb the small-sized PM, thus increasing the overall haze-holding capacity (Li et al., 2020). Since the pressure drop of the combined filter screen is still determined by the porosity of the main filter screen as well as the diameter of the pores, the increase in pressure drop is not significant, and the airflow rate in the chimney runner shows only a small decrease. Compared to increasing the thickness of the filter screen, employing a combination of filter screens made of different materials proves more effective in enhancing overall filtration efficiency while minimizing air resistance.

Fig. 15 summarizes the average filtration efficiency, pressure drop and airflow of the 13 filtration schemes. It can be found that the filtration efficiencies of the different materials of clean filter screens are positively correlated with the pressure drop they produce, and negatively correlated with the total clean air mass flow rate of the overflow clean filter screens during the test period. This makes the HEPA (C1), which has a high filtration efficiency of 93.1%, underperforms in total clean air mass flow rate, which is half of that of the nylon filter screen (C6), with a filtration efficiency of only 22.1%. This indicates that a high filtration efficiency and high pressure drop filter screen is not suitable for the 4m high solar chimney dust haze removal street light. Because the high pressure drop filter screen will significantly reduce the flow rate of the air in the chimney runner, which in turn significantly reduces the dust-haze containing airflow purified by the operation of the street light. In the table, C2, C9, C11

and C12 have good total clean air mass flow, in which low filtration efficiency filter screen such as activated carbon, nylon plus activated carbon combination filtration, although they had good permeability, but the filtration efficiency of 30% or so will lead to the solar chimney dust haze removal street light from the top of the chimney discharged most of the air still contains a large number of haze particles, and the excessive haze particles into the vertical heat collection area will pollute the chimney inner wall and reduce the solar irradiance transmittance. Therefore, it is necessary to measure the filtration efficiency of the purification and the pressure drop caused by them. Comprehensively comparing these 13 clean filtration solutions, the filter screen with medium filtration efficiency - primary filter cotton has the highest total clean air mass flow rate of 4.18 g, its filtration efficiency is 53.1%, and the pressure drop is only 0.339 Pa. Therefore, if the street light wants to get the highest total clean air mass flow rate, the single-layer 10mm thickness of primary filter cotton can be selected as the purification. For the street light to have the best air filtration efficiency, a single layer of 10mm HEPA can be chosen.

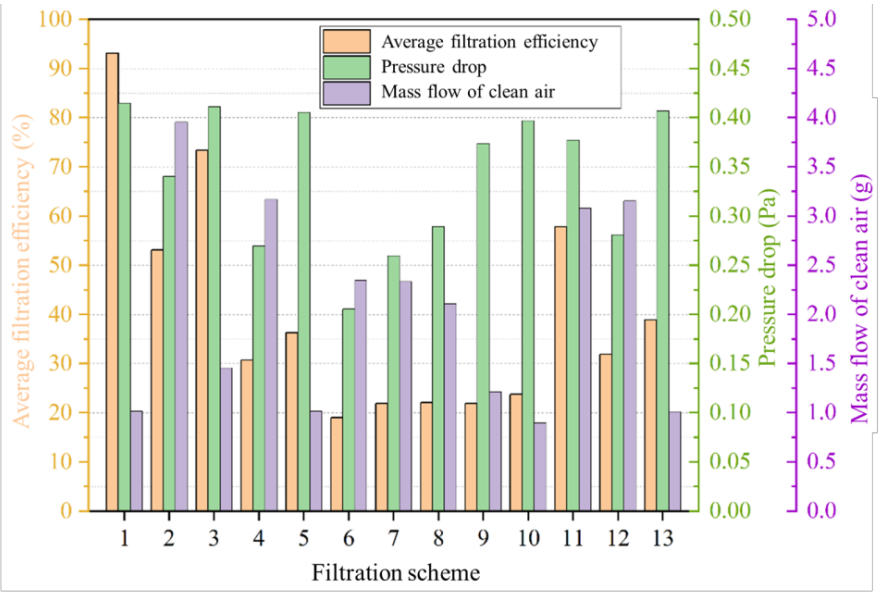

Fig. 15. Performance of different filtration schemes

5. Conclusion

This paper innovatively combines vertical solar chimney technology with municipal street lighting facilities, designing s a new type of solar chimney dust haze removal street light that integrates lighting and purification functions. This dust haze removal street light essentially maintains the original municipal lighting facilities on city roads, using solar and wind energy for dust haze removal, thus requiring no additional power consumption. It is easy to implement, noiseless, and environmentally

friendly. Based on the test prototype, a test model of small-scale test model of the solar chimney dust haze removal street light is built. Tests and analyses were conducted on the airflow characteristics and dust removal effects of the street light model under the actual atmospheric conditions. The effects of different filter materials, thicknesses and various combinations of filters on the performance of the street light purification were investigated. The main conclusions are as follows:

(1) The temperatures of the heat storage layer, the airflow in the runners, and the chimney wall all exhibit variations following a sinusoidal function law, as does the airflow velocity. The temperature of the heat storage layer reaches the peak value the latest, and its average temperature and peak temperature are much higher than that of the chimney wall and airflow. The minimum temperature of the heat storage layer was 1 to 2°C higher than the minimum ambient temperature, the heat storage layer can steadily supply heat to the airflow.

(2) The temperatures of the chimney wall, airflow and heat storage layer all increase and then decrease with height, peaks at one-eighth of the way from the chimney outlet. There are differences in the warming rate of airflow at different height levels, and the airflow warms up the most in the inlet region segment, where the heat absorption of the air is mainly concentrated. The highest temperature increase of the airflow in the runner in two days is 19.0℃ and 18.9℃, respectively. The solar chimney dust haze removal street light can create a rising hot airflow, and the chimney outlet may have backflow impeding the suction in the flow runner.

(3) Various filter screens are ranked from highest to lowest filtration efficiency as HEPA, primary filter cotton, activated carbon and nylon filter screens, while the size of the airflow rate in the chimney runner is ranked in the opposite order, and the filtration efficiency is inversely proportional to the air resistance it brings. The increase in the number of layers of the same type of filter screen brings about an increase in filtration efficiency that is far less than the decrease in the airflow rate in the chimney runners. A combination of different filter screens is more effective than increasing the thickness of a single filter screen.

(4) The average filtration efficiency of filter screens of different materials is positively correlated with the pressure drop it produces, and negatively correlated with the clean air mass flow rate of the overflow filter screen. 4m high solar chimney dust haze removal street light is not suitable for the use of high filtration efficiency and high pressure drop of the filter screen. Among the 13 clean filtration solutions, the total clean air mass flow rate of the primary filter cotton with a single layer of 10

mm thickness is the highest, reaching 4.18 g. The average filtration efficiency of the single-layer 10 mm HEPA is the highest, reaching 93.1%.

6. Acknowledgment

This research was financially supported by National Natural Science Foundation of China (No. 51976053).

7. Reference

Bagheri, S., Hassanabad, M.G., 2023. Numerical and experimental investigation of a novel vertical solar chimney power plant for renewable energy production in urban areas. Sustain. Cities Soc. 96, 104700. https://doi.org/10.1016/j.scs.2023.104700.

Bouchair, A., 2022. The effect of the altitude on the performance of a solar chimney. J. Energy. 249, 123704. https://doi.org/10.1016/j.energy.2022.123704.

Cao, Q.F., Pui, D.Y.H., Lipinski. W., 2015. A concept of a novel solar-assisted large-scale cleaning system (SALSCS) for urban air remediation, Aerosol. Air Qual. Res. 15 (1), 1-10. https://doi.org/10.4209/aaqr.2014.10.0246.

Cao, Q.F., Kuehn, T.H., Shen, L., Chen S.C., Zhang, N.N., Huang, Y., Cao, J.J., Pui, D.Y.H., 2018. Urban-scale SALSCS, Part I- Experimental Evaluation and Numerical Modeling of a Demonstration Unit. Aerosol. Air Qual. Res. 18(11), 2865–2878. https://doi.org/10.4209/aaqr.2018.06.0238.

Chen, Z.D., Bandopadhayay, P., Halldorsson, J., Byrjalesn, C., Heiselberg, P., Li, Y., 2003. An experimental investigation of a solar chimney model with uniform wall heat flux. Build. Environ. 38 (7), 893-906. https://doi.org/10.1016/S0360-1323(03)00057-X.

Chow, W.K., Zhao, J.H., 2011. Scale modeling studies on stack effect in tall vertical shafts. J. Fire Sci. 29 (6), 531-542. https://doi.org/10.1177/0734904111410657.

Gong, T.R., Ming, T.Z., Huang, X.M., Richter, D.R., Wu, Y.J., Liu, W., 2017. Numerical analysis on a solar chimney with an inverted U-type cooling tower to mitigate urban air pollution. Sol Energy. 147 (MAY), 68-82. https://doi.org/10.1016/j.solener.2017.03.030.

Haaf, W., Friedrich, K., Mayr, G., Schlaich, J., 2007. Solar chimneys Part I: Principle and Construction of the Pilot Plant in Manzanares. Int. J. Sol. Energy. 2, 3-20. https://doi.org/10.1080/01425918308909911.

Hachicha, A.A., Abo-Zahhad, E.M., Oh, S., Issa, S., Rahman, S.M.A., 2023. Numerical investigation and optimization of a novel hybrid solar chimney for air pollution mitigation and clean electricity generation. Appl. Therm. Engg. 226(226), 120271. https://doi.org/10.1016/j.applthermaleng.2023.120271.

Helmenstine, A.M., 2015. "The Relative Uncertainty Formula and How to Calculate It." Ph.D. ThoughtCo. https://www.thoughtco.com/definition-of-relative-uncertainty-605611 (accessed June 2, 2024).

Jing, H.W., Chen, Z.D., Li, A.G., 2015. Experimental study of the prediction of the ventilation flow rate through solar chimney with large gap-to-height ratios. Build. Environ. 89, 150-159. https://doi.org/10.1016/j.buildenv.2015.02.018.

Khanal, R., Lei, C.W., 2012. Flow reversal effects on buoyancy induced air flow in a solar chimney. Sol Energy. 86 (9), 2783-2794. https://doi.org/10.1016/j.solener.2012.06.015.

Khanal, R., Lei, C.W., 2014. An experimental investigation of an inclined passive wall solar chimney for natural ventilation, Sol Energy. 107 (9), 461–474. https://doi.org/10.1016/j.solener.2014.05.032.

Kurppa, M., Hellsten, A., Auvinen, M., Raasch, S., Vesala, T., Järvi, L., 2018. Ventilation and Air Quality in City Blocks Using Large-Eddy Simulation—Urban Planning Perspective. Atmosphere. 9 (2), 65. https://doi.org/10.3390/atmos9020065.

Li, A.G., Hao, C.X., Zhang, H.P., 2009. Experimental study on solar chimney for natural ventilation. Acta Energiae Sol Sinica. 30 (4), 5. https://doi.org/10.3321/j.issn:0254-0096.2009.04.011.

Li, L.Z., Wang, B., Zeng, J.S., 2020. Effect of glass fiber filter thickness on liquid filtration performance. J. China Pulp & Paper. 39 (05), 10-16. https://doi.org/10.11980/j.issn.0254-508X.2020.05.002.

Li, Y. C., 2011. "The experimental study of natural ventilation effect that under the action of solar ventilation technology combined with PCM," M.S. thesis, Dept. Chongqing University, Chongqing, China. https://doi.org/10.7666/d.y1663403.

Liu, Y., 2020. Research on filtration characteristic and preparation of micro/nano-fibrous mixed filtration materials. D. Tiangong University. https://doi.org/10.27357/d.cnki.gtgyu.2020.000505.

Liu, Y., Ming, T.Z., Peng, C., Wu, Y.J., Li, W., Richter, D.R., Zhou, N., 2021. Mitigating air pollution strategies based on solar chimneys. Sol. Energy. 218, 11-27. https://doi.org/10.1016/j.solener.2021.02.021.

Lodhi, M., 1999. Application of helio-aero-gravity concept in producing energy and suppressing pollution. Energy. Covers. Manag. 40 (4), 407-421. https://doi.org/10.1016/S0196-8904(98)00104-6.

Rattanongphisat, W., Imkong, P., Khunkong, S., 2017. An experimental investigation on the square steel solar chimney for building ventilation application. Energy Procedia. 138, 1165-1170. https://doi.org/10.1016/j.egypro.2017.10.226.

Ryan, D., Burek, S.A.M., 2010. Experimental study of the influence of collector height on the steady state performance of a passive solar air heater. Sol Energy. 84 (9), 1676-1684. https://doi.org/10.1016/j.solener.2010.05.018.

Spencer, S., 2001. "An experimental investigation of a solar chimney natural ventilation system," M.A.Sc. Concordia University, Montreal, Quebec, Canada. https://api.semanticscholar.org/CorpusID:107689150.

Yang, L., Li, Z., 2020. Mitigating air problems and producing renewable energy with solar downdraft tower. IOP Conf. Series Earth. Environ. Sci. 508(1), 012022. https://doi.org/10.1088/1755-1315/508/1/012022.

Yodo hotspot, 2018. 12 million to build a " dehaze tower " air filtration efficiency of 80% or more in Xian, EB/OL. https://www.sohu.com/picture/277749907 (accessed 1 April 2022).

Zhou, X.P., Xu, Y.Y., Yuan, S., Wu, C., Zhang, H., 2015. Performance and potential of solar updraft tower used as an effective measure to alleviate Chinese urban haze problem, Renew. Sustain. Energy Rev. 51(PT.899-1798), 1499-1508. https://doi.org/10.1016/j.rser.2015.07.020.

Zhou, Y., Wang, L., Gong, Y.Y., Lu, H.B., Dong, H.R., Li, Q.L., 2016. Study on the operation mechanism of vertical solar chimney power plant system. Acta Energiae Sol Sinica. 37 (11), 2868-2874. https://doi.org/10.19912/j.0254-0096.2016.11.021.

Zuo, L., Ding, L., Chen, J.J., Zhou, X.T., Xu, B.F., Liu, Z.H., 2018. Comprehensive study of wind supercharged solar chimney power plant combined with seawater desalination, Sol Energy. 166, 59-70. https://doi.org/10.1016/j.solener.2018.03.041.

Zuo, L., Zhou, T., Xu, C., Chen, S., Chen, Y., Liu, S.H., 2022. Research on PM_{10} diffusion and distribution of moving vehicle in street canyon based on dynamic mesh. Transp Eng. 10, 100151. https://doi.org/10.1016/j.treng.2022.100151.

Declaration of interests

☒ The authors declare that they have no known competing financial interests or personal relationships that could have appeared to influence the work reported in this paper.

☐ The authors declare the following financial interests/personal relationships which may be considered as potential competing interests: